PCCP

COMMUNICATION

View Article Online
View Journal | View Issue

Cite this: *Phys. Chem. Chem. Phys.*, 2016, **18**, 19536

Received 22nd April 2016,
Accepted 21st June 2016

DOI: 10.1039/c6cp02694j

www.rsc.org/pccp

Magnetoresistive polyaniline–silicon carbide metacomposites: plasma frequency determination and high magnetic field sensitivity†

Hongbo Gu,*[a] Jiang Guo,[b] Mojammel Alam Khan,[c] David P. Young,[c] T. D. Shen,[d] Suying Wei[e] and Zhanhu Guo*[b]

The Drude model modified by Debye relaxation time was introduced to determine the plasma frequency (ω_p) in the surface initiated polymerization (SIP) synthesized β-silicon carbide (β-SiC)/polyaniline (PANI) metacomposites. The calculated plasma frequency for these metacomposites with different loadings of β-SiC nanoparticles was ranging from 6.11×10^4 to 1.53×10^5 rad s^{-1}. The relationship between the negative permittivity and plasma frequency indicates the existence of switching frequency, at which the permittivity was changed from negative to positive. More interestingly, the synthesized non-magnetic metacomposites, observed to follow the 3-dimensional (3-D) Mott variable range hopping (VRH) electrical conduction mechanism, demonstrated high positive magnetoresistance (MR) values of up to 57.48% and high MR sensitivity at low magnetic field regimes.

Both electric permittivity (ε) and magnetic permeability (μ) are used to describe the propagation of an electromagnetic wave in a medium.[1] The materials with a negative refractive index (including negative ε and/or μ) at a certain frequency range are called metamaterials (known as left-handed media, LHM),[2,3] which were firstly introduced by Veselago in 1968.[4] Regular metamaterials are artificially constructed with special structures[5] and possess unique electromagnetic properties including reversed Doppler effect (normally, the Doppler effect predicts that the light shone by an observer onto an object moving toward him will be reflected by a medium with higher frequency. Reverse Doppler effect means that the light will be reflected by a medium with lower frequency[6]) and reversed Cherenkov radiation (Cherenkov radiation is emitted as charged particles moving with a speed faster than the phase velocity of light in the medium.[7] Veselago predicted that the reversed Cherenkov radiation allowed the backward emitted wave to be easily separated from the emitting charged particles[8]), antiparallel phase and group velocities, and backward power flow.[9] These special materials have received more attentions in the last few decades for their applications of optical cloaking, compact resonators, optical tunneling devices, subwavelength lenses and invisibility.[10,11]

Much more efforts have been made in the development of structured metamaterials, such as materials composed of an arrangement of resonant components,[12] non-resonant materials with an anisotropic response to DC magnetic fields,[10] composite structures consisting of ferrite layers (called wire medium, WM),[13] and doped-manganite-based structures.[14] Negative ε is one important key for developing metamaterials,[15] especially, the non-magnetic metamaterials, in which μ is 1.[16] Recently, the metallic (materials can be classified electronically into either insulating or metallic[17]) transport in conducting polymers and their nanocomposites has gained a lot of interest. The unique negative ε has been reported in polyaniline (PANI),[18] polypyrrole (PPy),[19] and their nanocomposites containing different nanofillers.[19–22] It is more important to understand the fundamentals of negative ε, which can help in the design of new metamaterials from the component rather than the structure controlled negative ε. More recently, a new term "metacomposites" was coined to describe the composites with negative ε, which is controlled by the component rather than the structure as in the conventional metamaterials.[23,24] Negative ε was observed in two types of nanocomposites. One is in the carbon nanofibers/elastomer nanocomposites[25] and graphene and its nanocomposites.[26] Another is in the conducting polymers including PPy[19,21,23] and PANI nanocomposites.[20,24,27] Meanwhile, the fundamentals of negative ε in PANI and its nanocomposites

[a] *Shanghai Key Lab of Chemical Assessment and Sustainability, Department of Chemistry, Tongji University, Shanghai, 200092, China. E-mail: hongbogu2014@tongji.edu.cn*
[b] *Integrated Composites Lab (ICL), Department of Chemical & Biomolecular Engineering, University of Tennessee, Knoxville, Tennessee, 37966, USA. E-mail: zguo10@utk.edu*
[c] *Department of Physics and Astronomy, Louisiana State University, Baton Rouge, LA 70803, USA*
[d] *State Key Laboratory of Metastable Materials Science and Technology, Yanshan University, Hebei 066004, China*
[e] *Department of Chemistry and Biochemistry, Lamar University, Beaumont, TX 77710, USA*

† Electronic supplementary information (ESI) available. See DOI: 10.1039/c6cp02694j

have been critically discussed by Gu *et al.*[28] Even though Lee *et al.*[29] reported the plasma frequency *via* the Drude model in metallic PANI, its application in the conducting polymer nanocomposites is not reported. Silicon carbide (SiC) is a unique ceramic semiconducting material with multifunctional properties[30] including a wide band gap from 2.4 to 3.2 eV, mechanical robustness, chemical resistivity, non-toxicity and biocompatibility, high thermal conductivity, low thermal expansion, and high refractive index,[31] allowing it to be used for novel electronic devices.[32] It is interesting to study the new functionalities after combining the conducting polymer PANI with semiconducting SiC.

Since the first discovery of the giant magnetoresistance (GMR) effect in the multilayer metallic thin-film structure consisting of ferromagnetic layers (Fe) separated by a non-magnetic metal layer (Cr) in 1988,[33,34] it has revolutionized the density of computer memory and storage industry by five orders of magnitudes.[35] In the last decade, GMR properties in the PANI nanostructures and nanocomposites have been reported.[36,37] For example, a large room temperature GMR up to 95% was reported in the magnetic PANI nanocomposites with a Fe_3O_4 nanoparticle loading of 30 wt%.[20] Meanwhile, the room temperature GMR effect was firstly reported in the non-magnetic PANI nanocomposites with nanofillers including silica,[38] $BaTiO_3$,[22] silicon,[39,40] different carbon nanostructures,[27] and WO_3.[41] In addition, the effects of oxidant, dosage of oxidant and doped acid on the GMR properties of PANI nanostructures were investigated.[20,38,42,43] However, the GMR properties of non-magnetic SiC/PANI nanocomposites have not been reported so far.

Herein, we report on the switching of ε from negative to positive and a large MR value with high sensitivity at low magnetic field regimes in *p*-toluene sulfonic acid (PTSA) doped β-SiC/PANI metacomposites. The plasma frequency (ω_p), relaxation time (τ), and damping constant (γ) were calculated *via* the Drude model modified by Debye relaxation time. The observed positive MR in the β-SiC/PANI metacomposites was analyzed by the wave-function shrinkage model.

The β-SiC/PANI nanocomposites were prepared by a surface initiated polymerization (SIP) method. The detailed experimental information is provided in the ESI.† The nanocomposites filled with a β-SiC loading of 10.0, 20.0, 40.0, and 60.0 wt% were prepared in this work. The observed characteristic peaks of PANI (1560, 1481, 1292, 1228, and 792 cm^{-1}), Fig. S1(f) and (b–e) (ESI†), confirm the conducting emeraldine salt (ES) form of PANI in these nanocomposites.[43] The diffraction peaks at around 2θ = 35.35, 40.95, 59.70, and 71.60° in the XRD curve of the as-received β-SiC nanoparticles and the PANI nanocomposites (Fig. S2, ESI†) correspond to the (1 1 1), (2 0 0), (2 2 0), and (3 1 1) crystallographic planes of moissanite SiC (standard XRD file PDF# 29-1129).[42] The broad peaks at around 20° and 25° in pure PANI, Fig. S2(f) (ESI†), are attributed to the (1 0 0) and (1 1 0) crystallographic planes of the partially crystallized PANI.[44] The intensity of these broad peaks decreases with increasing the β-SiC nanoparticle loading and disappears in the PANI nanocomposites with 60.0 wt% β-SiC, Fig. S2(e) (ESI†). The thermal stability of the β-SiC/PANI nanocomposites is observed to be higher than that of pure PANI and increases with increasing the β-SiC nanoparticle loading, Fig. S3 (ESI†).

Fig. 1 shows the angular frequency (ω) dependent real permittivity (ε'), imaginary permittivity (ε'') and dielectric loss ($\tan\delta$, where $\tan\delta = \varepsilon''/\varepsilon'$) of the PANI nanocomposites with different β-SiC loadings at room temperature within the measured angular frequency range of 1.26×10^2 to 1.26×10^7 rad s^{-1}. All the prepared nanocomposites show negative ε' values within the angular frequency range of 1.26×10^2 to 3.14×10^3 rad s^{-1} and then become positive as the angular frequency increases further, Fig. 1(A). The switching of ε' from negative to positive is also reported in the WO_3/PANI nanocomposites (which could be tuned by controlling the loading and morphology of the WO_3 nanostructures)[23] and multi-walled carbon nanotube (MWNTs)/PANI nanocomposites.[43] It is totally different from the pure PANI (Fig. S5, ESI†) in which the negative permittivity is observed within the whole measured angular frequency range. Generally, the dielectric properties of PANI are related to the intrinsic metallic nature in PANI such as conductivity and charge delocalization. The negative ε in PANI is normally due to the formation of a continuous conductive network in the polymer chains (or called metallic behavior).[45] At the angular frequency of 1.26×10^2 rad s^{-1}, the ε' of the β-SiC/PANI nanocomposites follows the trend: 10.0 wt% β-SiC (-6.61×10^2) > 40.0 wt% β-SiC (-1.38×10^3) > 20.0 wt% β-SiC (-3.27×10^3) > 60.0 wt% β-SiC (-1.06×10^4). The inset of Fig. 1(A) shows a positive ε' value within the frequency range from 1.7×10^4 to 1.7×10^7 rad s^{-1}. As the angular frequency is higher than 10^6 rad s^{-1}, the ε' of the β-SiC/PANI nanocomposites obeys the relationship: 10.0 wt% β-SiC > 60.0 wt% β-SiC > 20.0 wt% β-SiC > 40.0 wt% β-SiC. At higher angular frequency range (around 10^6–10^7 rad s^{-1}), the ε' experiences a decrease arising from the dielectric relaxation phenomenon,[24] which is caused by the decay of the molecular polarization in an alternative electric field.[19] Fig. 1(B) shows the ε'' of the β-SiC/PANI nanocomposites within the angular frequency range from 1.26×10^2 to 1.26×10^7 rad s^{-1}. The PANI nanocomposites with 60.0 wt% β-SiC loading exhibit the largest negative ε'' value among all the β-SiC/PANI nanocomposites at 125.7 rad s^{-1}. The switching frequency from negative to positive is also observed in the ε'', and the ε'' increases with the increasing ω ($<10^4$ rad s^{-1}) and then decreases obviously as ω increases further, inset of Fig. 1(B). Generally, this switching frequency is related to a unique frequency, which is called plasma frequency, ω_p.[46]

Normally, the free electrons, which behave like a plasma (as the scale of a solid is much larger than the inter atomic distance, a solid can serve as an aggregate consisting of a negatively charged plasma of the free electron gas and a positively charged background of atomic cores) with dielectric properties (as far as electromagnetic wave is concerned), dominate the interaction of light with a metal surface.[47] The collective oscillation of surface plasmons in a solid or liquid stimulated by an incident light is called surface plasmon resonance (SPR).[48] The Drude model, a simple classical conductivity model, is often used to describe the

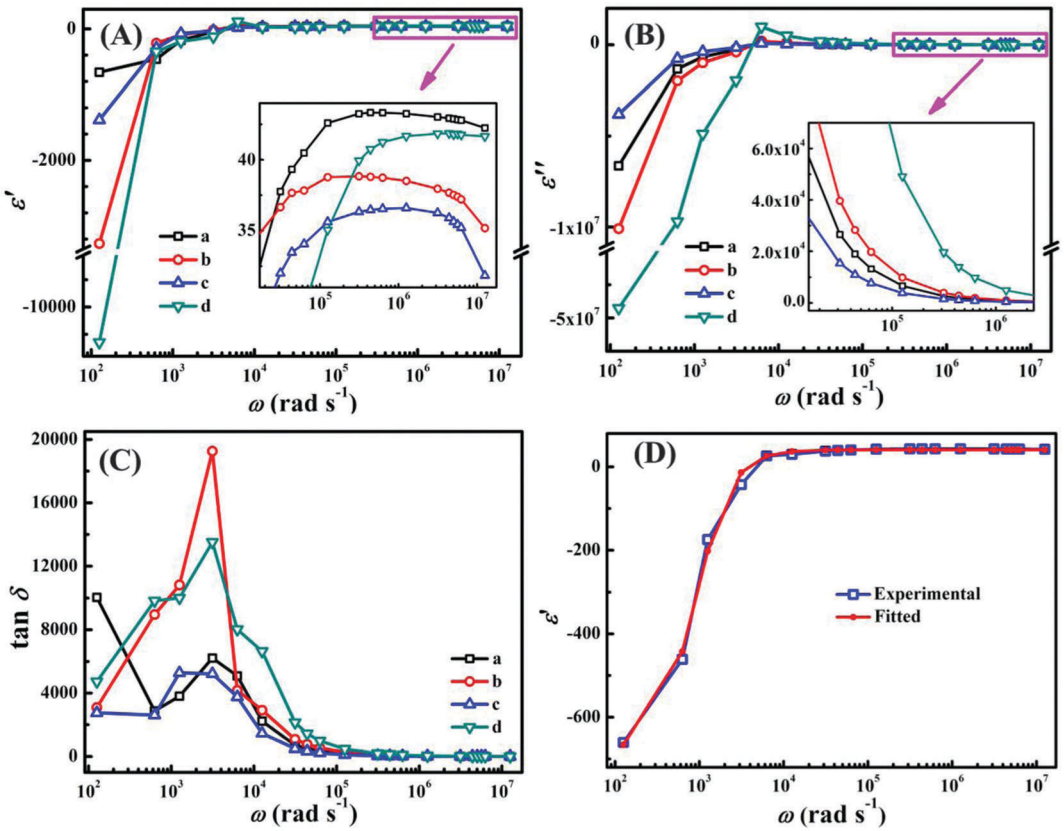

Fig. 1 (A) Real permittivity (ε'); (B) imaginary permittivity (ε''); and (C) dielectric loss ($\tan\delta$) as a function of angular frequency of PANI nanocomposites with a β-SiC loading of (a) 10.0, (b) 20.0, (c) 40.0 and (d) 60.0 wt%; insets of (A) and (B) show the enlarged ε' and ε'' change at the higher frequency range, respectively. (D) Experimentally measured and calculated ε' as a function of angular frequency for 10.0 wt% β-SiC/PANI.

existence and properties of surface plasmons by the frequency dependent permittivity between the external dielectric medium and the surface.[48] This permittivity is negative below the ω_p.[47] In the Drude model, the permittivity is dominated by the plasma-like resonance of the free electrons in a metal and shown in eqn (1):[49]

$$\varepsilon^*(\omega) = 1 - \frac{{\omega_p}^2}{\omega(\omega + i\gamma)} \quad (1)$$

where $\omega_p \equiv (Ne^2/\varepsilon_0 m)^{1/2} = (4\pi Ne^2/m^*)^{1/2}$ is plasma frequency, m is the mass of an electron, m^* is the optical effective mass of electron, γ stands for the damping constant (which is from the damping force; normally, all the oscillators have damping, such as fluid drag), ε_0 is the vacuum permittivity, e is electron charge, N represents the charge carrier density and ω is angular frequency of the incident light.[50,51] However, the earliest results showed that the Drude's free electron theory did not fit the experimental results in the visible and near-ultraviolet regions.[52] Normally, in the quantum theory, the absorption in the visible and ultraviolet regions may be due to the transition from the filled d bands to the sp conduction bands.[52] In order to fit the optical data on the metals in these regions, the Debye relaxation time τ (which describes the response of electric dipoles to an alternating electric field and the essential dynamics is expressed by the exponential relation (i/τ) of the dipole polarization with time[53]) is introduced to modify the Drude model to interpret the frequency dependent permittivity property as eqn (2):[52,54]

$$\varepsilon^*(\omega) = 1 - \frac{{\omega_p}^2}{\omega(\omega + i\gamma)} = 1 - \frac{{\omega_p}^2}{\omega(\omega + i/\tau)} = \left(1 - \frac{{\omega_p}^2\tau^2}{1 + \omega^2\tau^2}\right) + i\left(\frac{{\omega_p}^2\tau}{\omega(1 + \omega^2\tau^2)}\right) \quad (2)$$

where τ is the electron relaxation time and $\tau = 1/\gamma$. In eqn (2), the real part of the permittivity (expressed as: $1 - {\omega_p}^2\tau^2/(1 + \omega^2\tau^2)$) is observed to be negative for $\omega < \omega_p$, which means that when ω is lower than ω_p, the charges can move quickly to shield the interior of the medium from the electromagnetic radiation and when ω is larger than ω_p, the medium behaves as an ordinary dielectric medium.[55] As angular frequency becomes larger, the $1/\omega^2$ dependence of the free carrier contribution (which is expressed as $(4\pi i/\omega) \times (N\tau/(m^*(1 - i\omega\tau)))$) makes the free carrier contribution less important. Therefore, in the Debye dielectric relaxation, the high frequency limit ε_∞ (appropriated to electronic excitation processes since the relaxation is related to the excited states of excited species or absorbed atoms and molecules[56]) is often introduced to express the optical dielectric

properties when discussing the electronic process investigated using the optical techniques, and eqn (2) becomes eqn (3):[29]

$$\varepsilon^*(\omega) = \varepsilon_\infty - \frac{\Omega_p^2}{\omega(\omega + i/\tau)} = \left(\varepsilon_\infty - \frac{\Omega_p^2\tau^2}{1+\omega^2\tau^2}\right) + i\left(\frac{\Omega_p^2\tau}{\omega(1+\omega^2\tau^2)}\right) \quad (3)$$

where Ω_p is the screened electronic plasma frequency and $\Omega_p = \omega_p/(\varepsilon_\infty)^{1/2}$.[29] The investigation of plasma frequency ω_p and other parameters including relaxation time τ, charge carrier density N, and high frequency limit permittivity ε_∞ using the Drude model is beneficial for the development of new metamaterials.

Fig. 1(D) shows the ω dependent real permittivity $\varepsilon'(\omega)$ of the 10.0 wt% β-SiC PANI nanocomposites at room temperature. The $\varepsilon'(\omega)$ is fitted using the real part of the Drude model from eqn (3): $\varepsilon'(\omega) = \varepsilon_\infty - \Omega_p^2\tau^2/(1+\omega^2\tau^2)$, with the assistance of a non-linear fitting by using the Polymath software (which is commonly used to obtain the constant parameters in the equation through non-linear fitting). The fitting results are illustrated in Fig. 1(D). The fitting coefficient is 0.9969 and the obtained fitting parameters including ε_∞, τ and Ω_p are shown in Table 1. The obtained Ω_p value for the β-SiC/PANI nanocomposites is 2.40×10^4 rad s^{-1} (= 3.83×10^3 Hz = 1.28×10^{-5} m^{-1}) and $\tau = 1.11 \times 10^{-3}$ s with a high frequency dielectric constant $\varepsilon_\infty = 40.63$. According to the expression of the real part in eqn (3), $\varepsilon'(\omega)$ crosses zero and becomes positive at the Ω_p value of 2.40×10^4 rad s^{-1}, which means that the permittivity remains negative at all frequencies below 2.40×10^4 rad s^{-1}. The relationship between negative real permittivity and plasma frequency indicates the switching of real permittivity from negative to positive. Thus, the plasma frequency ω_p calculated from $\Omega_p = \omega_p/(\varepsilon_\infty)^{1/2}$ is 1.53×10^5 rad s^{-1} (= 2.43×10^4 Hz = 8.13×10^{-5} m^{-1}) and the damping constant γ (=$1/\tau$) is 9.01×10^2 s^{-1}. With the obtained ω_p, the charge carrier density N calculated from $\omega_p = (Ne^2/\varepsilon_0 m)^{1/2}$ is 7.39×10^6 m^{-3}. These parameters calculated from the Drude model fit are reasonable and consistent with the previous report on the metallic PANI structures.[29] The fitting parameters for β-SiC/PANI nanocomposites with other loadings of β-SiC nanoparticles are shown in Table 1 and Fig. S5 (ESI†). It is observed that the nanoparticle loading of β-SiC/PANI nanocomposites has an effect on the parameters of the nanocomposites.

Fig. 1(C) depicts the ω dependent $\tan\delta$ for the β-SiC/PANI nanocomposites. The $\tan\delta$ of these prepared samples increases with increasing the ω ($< 3.1 \times 10^3$ rad s^{-1}) and then decreases sharply by 3–4 orders of magnitudes as ω increases further. A peak, observed in the $\tan\delta$ curves of the β-SiC/PANI nanocomposites, corresponds to the switching frequency from negative to positive due to the induced polarization at high ω.[23] This is also observed in the WO_3/PANI,[24] WO_3/PPy,[23] and MWNTs/PANI nanocomposites.[43]

The temperature dependent resistivity of the PANI nanocomposites with different β-SiC nanoparticle loadings is measured from 50 to 290 K, Fig. 2(A). All the prepared samples exhibit a semiconducting behavior within the measured temperature range with the resistivity decreasing with increasing the temperature.[57] The resistivity of 10.0 wt% β-SiC/PANI nanocomposites changes from 5.4×10^5 Ω cm (50 K) to 2.5×10^2 Ω cm (290 K). The resistivity of 20.0 wt% β-SiC nanocomposites varies from 6.1×10^5 Ω cm (50 K) to 3.0×10^2 Ω cm (290 K). The resistivity of 40.0 wt% β-SiC nanocomposites changes from 7.4×10^5 Ω cm (50 K) to 3.9×10^2 Ω cm (290 K). And the resistivity of 60.0 wt% β-SiC nanocomposites changes from 2.7×10^5 Ω cm (50 K) to 80.58 Ω cm (290 K). In summary, the resistivity of the nanocomposites increases as the β-SiC loading increases to 40.0 wt%, after that the resistivity decreases as the β-SiC loading increases to 60.0 wt%. This indicates that the loading of β-SiC nanoparticles can affect the resistivity of the nanocomposites, which is also observed in the silicon/PANI nanocomposites.[39] It is well known that SiC is a wide bandgap semiconductor for applications in high-voltage and high-power electronics.[58] The high loading of semiconducting SiC nanoparticles may provide more charge carrier for the conduction, leading to the decreased resistivity of 60.0 wt% β-SiC/PANI nanocomposites.

The electrical transport behavior of these nanocomposites is explored using the Mott variable range hopping (VRH) approach. The VRH approach describes that when the electrons are localized near the Fermi energy, they can hop from one site to other sites that are separated spatially by different distances after neglecting the Coulomb repulsion in the disordered materials.[59,60] The temperature dependent electrical conductivity ($\sigma(T)$) in the VRH regime is expressed as eqn (4):[39]

$$\sigma(T) = \sigma_0 \exp\left[-\left(\frac{T_0}{T}\right)^{\frac{1}{n+1}}\right] \quad (4)$$

where σ_0 is a constant, standing for the conductivity at an infinitely low temperature, T is the Kelvin temperature, and the constant T_0 (K) is the Mott characteristic temperature, which is related to the energy needed for the hopping conduction of the charge carriers and given by eqn (5):[61]

$$T_0 = 24/[\pi k_B N(E_F) a_0^3] \quad (5)$$

where a_0 (nm) is the localization length of the localized wavefunction of charge carriers, k_B is Boltzmann constant and

Table 1 Calculated Ω_p, ω_p, ε_∞, τ, γ, and N for the β-SiC/PANI nanocomposites

Samples	Ω_p (rad s^{-1})	ω_p (rad s^{-1})	ε_∞	τ (s)	γ (s^{-1})	N (m^{-3})
β-SiC/PANI						
10.0 wt%	2.40×10^4	1.53×10^5	40.63	1.11×10^{-3}	9.01×10^2	7.39×10^6
20.0 wt%	1.06×10^4	6.11×10^4	33.33	7.42×10^{-3}	1.35×10^2	1.18×10^6
40.0 wt%	1.28×10^4	7.12×10^4	31.12	3.17×10^{-3}	3.15×10^2	1.60×10^6
60.0 wt%	1.30×10^4	7.08×10^4	29.75	8.93×10^{-4}	1.12×10^3	1.58×10^6

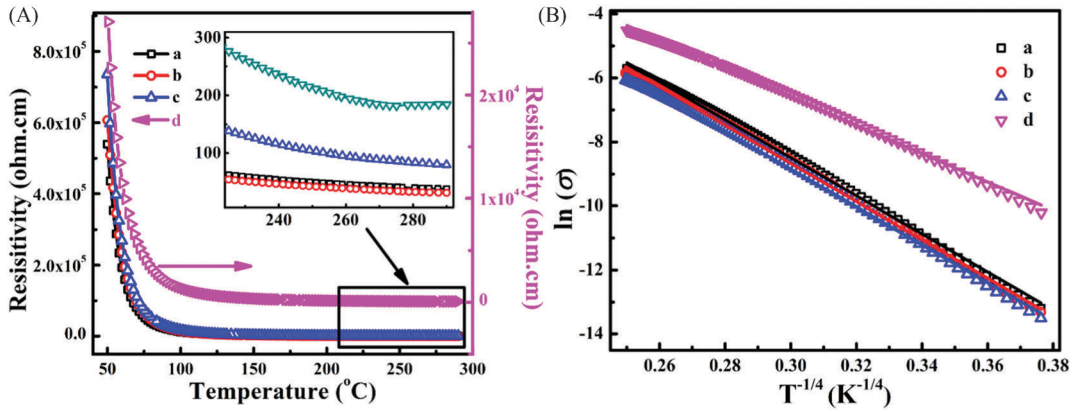

Fig. 2 (A) Resistivity as a function of temperature, (B) ln(σ) as a function of $T^{-1/4}$ for PANI nanocomposites with a β-SiC loading of (a) 10.0, (b) 20.0, (c) 40.0, and (d) 60.0 wt%. The inset of (A) shows the enlarged resistivity change at a higher temperature range.

$N(E_F)$ (eV cm^3)$^{-1}$ is the density of states at the Fermi level. Normally, in the disordered system, the localized wave-function of the charge carrier means that both the phase and amplitude of the wave-function are fluctuated by the interference effect, which forces the wave-function to exponentially decay to zero for very large distances. The localization length is used to characterize this decay and is defined through the logarithmic average of the absolute value of the wave-function.[62] Eqn (5) indicates that T_0 is related to both $N(E_F)$ and a_0. In the Mott VRH mechanism, the average hopping distance (R_{hop}, which is the average nearest-neighbour "distance" between states), and average hopping energy (W) can be expressed as eqn (6) and (7), respectively:

$$R_{hop} = (3/8)(T_0/T)^{\frac{1}{4}} a_0 \quad (6)$$

$$W = \frac{3}{4\pi R_{hop}{}^3 N(E_F)} \quad (7)$$

The n value in eqn (4) is related to the dimensionality of the conduction process and n = 3, 2, and 1 for 3-, 2-, and 1-dimensional system, respectively.[63] The σ_0 and T_0 values can be obtained from the intercept and slope of the plot $\ln(\sigma) \sim T^{-1/(n+1)}$, respectively. The best linear fit of $\ln(\sigma) \sim T^{-1/(n+1)}$ (obtained from Fig. 2(A)) is plotted in Fig. 2(B). The PANI nanocomposites with different β-SiC nanoparticle loadings are observed to linearly follow the relationship: $\ln(\sigma) \sim T^{-1/4}$, indicating a quasi 3-d VRH electrical transport mechanism. The obtained σ_0 and T_0 values from Fig. 2(B) are summarized in Table 2. The σ_0 of the β-SiC/PANI nanocomposites is observed to decrease with increasing the β-SiC nanoparticle loading. The 60.0 wt% β-SiC/PANI nanocomposites show the lowest T_0 among the prepared nanocomposites, which means that it requires the lowest energy for the hopping of charge carriers. This is consistent with the decreased resistivity for 60.0 wt% β-SiC/PANI nanocomposites as aforementioned.

MR, the resistance change of a material after applying an external magnetic field, is defined as eqn (8):

$$MR\% = \frac{\Delta R}{R} = \frac{R(H) - R(0)}{R(0)} \times 100 \quad (8)$$

Table 2 T_0 and σ_0 for the β-SiC/PANI nanocomposites

Samples	$T_0 \times 10^7$ (K)	σ_0 (S cm^{-1})
Pure PANI[20]	0.70	1826.00
10.0 wt% β-SiC/PANI	1.25	11279.81
20.0 wt% β-SiC/PANI	1.27	10399.26
40.0 wt% β-SiC/PANI	1.21	7012.64
60.0 wt% β-SiC/PANI	0.39	852.39

where $R(0)$ and $R(H)$ are the resistance at zero and any applied magnetic field H, respectively. The room temperature MR values of the nanocomposites with different β-SiC nanoparticle loadings are shown in Fig. 3. The MR for all the samples is observed to be positive within the whole measured magnetic field and increases with increasing the applied magnetic field. The room temperature MR of the PTSA doped pure PANI is observed to be 53% at a magnetic field of 9 T in our previous work.[20] The room temperature MR value of the PANI nanocomposites with a β-SiC nanoparticle loading of 10.0, 20.0, 40.0,

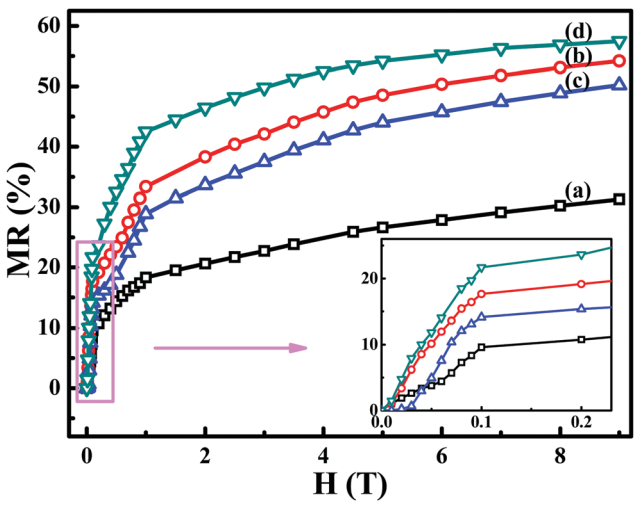

Fig. 3 Room temperature MR of the PANI nanocomposites with a β-SiC loading of (a) 10.0, (b) 20.0, (c) 40.0, and (d) 60.0 wt%. The inset shows the enlarged MR signal at the low magnetic field.

and 60.0 wt% is 31.27, 54.18, 50.19, and 57.48% at magnetic field of 9 T, respectively. The MR value at room temperature of the β-SiC/PANI nanocomposites has the magnetic field dependent property and increases with increasing the magnetic field. The slope of MR curves at low magnetic fields indicates the MR sensitivity of the materials to an external magnetic field.[64] The slope of MR curves for the nanocomposites with a β-SiC nanoparticle loading of 10.0, 20.0, 40.0 and 60.0 wt% is 87.10, 201.94, 185.63, and 220.48, respectively, which is higher than that of pure PANI (around 40.93). The obtained MR sensitivity obeys the following relationship: pure PANI < 10.0 wt% β-SiC/PANI < 40.0 wt% β-SiC/PANI < 20.0 wt% β-SiC/PANI < 60.0 wt% β-SiC/PANI.

Normally, the MR can be determined using the wave-function shrinkage model under a weak magnetic field regime (considering the studied non-magnetic materials, the used field is still considered as weak) as described by eqn (9):[65]

$$\mathrm{MR} = \frac{R(H,T) - R(0,T)}{R(0,T)} \approx t_2 \frac{H^2}{P_C{}^2}\left(\frac{T_0}{T}\right)^{\frac{1}{4}} \quad (9)$$

where the numerical constant t_2 = 5/2016[66] and H is the magnetic field, P_C is the fitting parameter given by eqn (10) for the 3-d Mott VRH electrical transport mechanism.

$$P_C = 6\hbar/[e{a_0}^2(T_0/T)^{1/4}] \quad (10)$$

According to eqn (9), the localization length a_0 can be obtained from eqn (11).

$${a_0}^4 = \frac{36\hbar^2\mathrm{MR}}{t_2 e^2}\left(\frac{T_0}{T}\right)^{-\frac{3}{4}} H^{-2} \quad (11)$$

For example, T_0 is 1.25 × 10^7 K for the nanocomposites with a β-SiC nanoparticle loading of 10.0 wt%, and the calculated a_0 from eqn (11) at room temperature is 72.3, 27.9 and 20.7 nm at H of 0.5, 4 and 9 T, respectively. The calculated a_0 values of the nanocomposites with different β-SiC loadings are shown in Table 3. It is seen that a_0 has different values under different H. After obtaining a_0, the $N(E_F)$ can be calculated from eqn (12):

$$N(E_F) = 24/[\pi k_B T_0 {a_0}^3] \quad (12)$$

and the calculated results are listed in Table 3. The $N(E_F)$ is observed to increase with increasing the H. The calculated average hopping distance R_{hop} and average hopping energy W according to eqn (6) and (7) are also shown in Table 3, respectively. It is observed that R_{hop} (nm) is H dependent and decreases with increasing H, which means that the average nearest-neighbor "distance" between states is affected by H and decreases with increasing H. However, the calculated W is observed to be constant under different H, which is also observed in the WO_3/PANI nanocomposites.[41] This means that the energy needed for the charge carrier hopping process for these nanocomposites is independent of the magnetic field H.

In conclusion, the Drude model modified by Debye relaxation time is used to determine ω_p, τ, γ, ε_∞, and N of the β-SiC/PANI metacomposites prepared through a SIP method. The β-SiC loading has an effect on the above parameters. These obtained parameters would be very helpful in understanding the fundamentals of negative ε and the design of conducting polymer based metamaterials. The investigation of these parameters is useful for the development of high-performance semiconducting and metallic polymers in the "plastic electronics" for other possible applications.[29] High MR sensitivity at low magnetic field regimes and high positive MR values are observed in these non-magnetic β-SiC/PANI metacomposites, making them possess

Table 3 a_0, $N(E_F)$, R_{hop} and W for pure PANI doped with PTSA and its β-SiC nanocomposites at different magnetic fields H

		Magnetic field H (T)		
Samples	Parameters	0.5	4.5	9
PTSA doped pure PANI	a_0 (nm)	39.6	17.1	12.1
	$N(E_F)$ (eV cm^3)$^{-1}$	2.04 × 10^{14}	2.50 × 10^{15}	7.23 × 10^{15}
	R_{hop} (nm)	184.9	80.3	56.3
	W (meV)	184.8	184.8	184.8
10.0 wt% β-SiC/PANI	a_0 (nm)	72.3	27.9	20.7
	$N(E_F)$ (eV cm^3)$^{-1}$	1.88 × 10^{13}	3.25 × 10^{14}	7.98 × 10^{14}
	R_{hop} (nm)	390.8	150.9	111.9
	W (meV)	213.6	213.6	213.6
20.0 wt% β-SiC/PANI	a_0 (nm)	81.9	32.6	23.8
	$N(E_F)$ (eV cm^3)$^{-1}$	1.27 × 10^{13}	2.02 × 10^{14}	5.16 × 10^{14}
	R_{hop} (nm)	444.5	176.7	129.2
	W (meV)	214.4	214.2	214.2
40.0 wt% β-SiC/PANI	a_0 (nm)	76.9	31.5	23.2
	$N(E_F)$ (eV cm^3)$^{-1}$	1.61 × 10^{13}	2.35 × 10^{14}	5.90 × 10^{14}
	R_{hop} (nm)	412.0	168.6	124.1
	W (meV)	211.8	157.8	157.8
60.0 wt% β-SiC/PANI	a_0 (nm)	71.3	26.9	19.4
	$N(E_F)$ (eV cm^3)$^{-1}$	6.26 × 10^{19}	1.16 × 10^{21}	3.12 × 10^{21}
	R_{hop} (nm)	288.0	108.7	78.3
	W (meV)	159.6	159.6	159.6

potential for application in magnetic field sensors, biosensors, and biochip systems.

Acknowledgements

This work was supported by the Shanghai Science and Technology Commission (14DZ2261100), a start-up fund from the University of Tennessee, and the Science and Technology Commission of Shanghai Municipality (No. 15YF1412700) and Program for Young Excellent Talents in Tongji University (No. 2014KJ028). D. P. Young acknowledges the support from the National Science Foundation (DMR 1306392).

Notes and references

1 Y. Yao and X. Zhao, *J. Appl. Phys.*, 2007, **101**, 124904.
2 J. Valentine, S. Zhang, T. Zentgraf, E. Ulin-Avila, D. A. Genov, G. Bartal and X. Zhang, *Nature*, 2008, **455**, 376–379.
3 V. M. Shalaev, *Nat. Photonics*, 2007, **1**, 41–48.
4 V. G. Veselago, *Phys.-Usp.*, 1968, **10**, 509–514.
5 R. W. Ziolkowski and E. Heyman, *Phys. Rev. E: Stat., Nonlinear, Soft Matter Phys.*, 2001, **64**, 056625.
6 E. J. Reed, M. Soljačić and J. D. Joannopoulos, *Phys. Rev. Lett.*, 2003, **91**, 133901.
7 Z. Duan, B.-I. Wu, S. Xi, H. Chen and M. Chen, *Prog. Electromagn. Res.*, 2009, **90**, 75–87.
8 S. Xi, H. Chen, T. Jiang, L. Ran, J. Huangfu, B.-I. Wu, J. A. Kong and M. Chen, *Phys. Rev. Lett.*, 2009, **103**, 194801.
9 K. L. Tsakmakidis, C. Hermann, A. Klaedtke, C. Jamois and O. Hess, *Phys. Rev. B: Condens. Matter Mater. Phys.*, 2006, **73**, 085104.
10 F. Magnus, B. Wood, J. Moore, K. Morrison, G. Perkins, J. Fyson, M. Wiltshire, D. Caplin, L. Cohen and J. Pendry, *Nat. Mater.*, 2008, **7**, 295–297.
11 J. Yao, Z. Liu, Y. Liu, Y. Wang, C. Sun, G. Bartal, A. M. Stacy and X. Zhang, *Science*, 2008, **321**, 930.
12 D. Schurig, J. Mock and D. Smith, *Appl. Phys. Lett.*, 2006, **88**, 041109.
13 H. Zhao, J. Zhou, Q. Zhao, B. Li, L. Kang and Y. Bai, *Appl. Phys. Lett.*, 2007, **91**, 131107.
14 M. Khodzitsky, S. Tarapov, D. Belozorov, A. Pogorily, A. Tovstolytkin, A. Belous and S. Solopan, *Appl. Phys. Lett.*, 2010, **97**, 131912.
15 C.-H. Hsieh, A.-H. Lee, C.-D. Liu, J.-L. Han, K.-H. Hsieh and S.-N. Lee, *AIP Adv.*, 2012, **2**, 012127.
16 V. A. Podolskiy and E. E. Narimanov, *Phys. Lett. B*, 2005, **71**, 201101.
17 M. I. Redondo and C. B. Breslin, *Corros. Sci.*, 2007, **49**, 1765–1776.
18 X. Zhang, J. Zhu, N. Haldolaarachchige, J. Ryu, D. P. Young, S. Wei and Z. Guo, *Polymer*, 2012, **53**, 2109–2120.
19 J. Guo, H. Gu, H. Wei, Q. Zhang, N. S. Haldolaarachchige, Y. Li, D. P. Young, S. Wei and Z. Guo, *J. Phys. Chem. C*, 2013, **117**, 10191–10202.
20 H. Gu, Y. Huang, X. Zhang, Q. Wang, J. Zhu, L. Shao, N. Haldolaarachchige, D. P. Young, S. Wei and Z. Guo, *Polymer*, 2012, **53**, 801–809.
21 J. Zhu, X. Zhang, N. Haldolaarachchige, Q. Wang, Z. Luo, J. Ryu, D. P. Young, S. Wei and Z. Guo, *J. Mater. Chem.*, 2012, **22**, 4996–5005.
22 X. Zhang, S. Wei, N. Haldolaarachchige, H. A. Colorado, Z. Luo, D. P. Young and Z. Guo, *J. Phys. Chem. C*, 2012, **116**, 15731–15740.
23 J. Zhu, S. Wei, L. Zhang, Y. Mao, J. Ryu, P. Mavinakuli, A. B. Karki, D. P. Young and Z. Guo, *J. Phys. Chem. C*, 2010, **114**, 16335–16342.
24 J. Zhu, S. Wei, L. Zhang, Y. Mao, J. Ryu, A. B. Karki, D. P. Young and Z. Guo, *J. Mater. Chem.*, 2011, **21**, 342–348.
25 J. Zhu, S. Wei, J. Ryu and Z. Guo, *J. Phys. Chem. C*, 2011, **115**, 13215–13222.
26 J. Zhu, Z. Luo, S. Wu, N. Haldolaarachchige, D. P. Young, S. Wei and Z. Guo, *J. Mater. Chem.*, 2012, **22**, 835–844.
27 J. Zhu, H. Gu, Z. Luo, N. Haldolaarachige, D. P. Young, S. Wei and Z. Guo, *Langmuir*, 2012, **28**, 10246–10255.
28 H. Gu, J. Guo, S. Wei and Z. Guo, *J. Appl. Polym. Sci.*, 2013, **130**, 2238–2244.
29 K. Lee, S. Cho, S. H. Park, A. J. Heeger, C. W. Lee and S. H. Lee, *Nature*, 2006, **44**, 65–68.
30 P. Mavinakuli, S. Wei, Q. Wang, A. B. Karki, S. Dhage, Z. Wang, D. P. Young and Z. Guo, *J. Phys. Chem. C*, 2010, **114**, 3874–3882.
31 H. Lin, J. A. Gerbec, M. Sushchikh and E. W. McFarland, *Nanotechnology*, 2008, **19**, 325601.
32 R. Yakimova, R. M. P. Jr, G. R. Yazdi, C. Vahlberg, A. L. Spetz and K. Uvdal, *J. Phys. D: Appl. Phys.*, 2007, **40**, 6435–6442.
33 M. N. Baibich, J. M. Broto, A. Fert, F. N. Van Dau, F. Petroff, P. Etienne, G. Creuzet, A. Friederich and J. Chazelas, *Phys. Rev. Lett.*, 1988, **61**, 2472.
34 G. Binasch, P. Grünberg, F. Saurenbach and W. Zinn, *Phys. Rev. B: Condens. Matter Mater. Phys.*, 1989, **39**, 4828–4830.
35 W. J. Gallagher and S. S. P. Parkin, *IBM J. Res. Dev.*, 2006, **50**, 5–23.
36 H. Gu, J. Guo, X. Yan, H. Wei, X. Zhang, J. Liu, Y. Huang, S. Wei and Z. Guo, *Polymer*, 2014, **55**, 4405–4419.
37 Y. Long, K. Huang, J. Yuan, D. Han, L. Niu, Z. Chen, C. Gu, A. Jin and J. L. Duvail, *Appl. Phys. Lett.*, 2006, **88**, 162113.
38 H. Gu, J. Guo, X. Zhang, Q. He, Y. Huang, H. A. Colorado, N. S. Haldolaarachchige, H. L. Xin, D. P. Young, S. Wei and Z. Guo, *J. Phys. Chem. C*, 2013, **117**, 6426–6436.
39 H. Gu, J. Guo, H. We, Y. Huang, C. Zhao, Y. Li, Q. Wu, N. Haldolaarachchige, D. P. Young, S. Wei and Z. Guo, *Phys. Chem. Chem. Phys.*, 2013, **15**, 10866–10875.
40 H. Gu, J. Guo, R. Sadu, Y. Huang, N. Haldolaarachchige, D. Chen, D. P. Young, S. Wei and Z. Guo, *Appl. Phys. Lett.*, 2013, **102**, 212403.
41 H. Gu, J. Guo, H. Wei, X. Zhang, J. Zhu, L. Shao, Y. Huang, N. Haldolaarachchige, D. P. Young, S. Wei and Z. Guo, *Polymer*, 2014, **55**, 944–950.
42 H. Gu, H. Wei, J. Guo, N. Haldolaarachige, D. P. Young, S. Wei and Z. Guo, *Polymer*, 2013, **54**, 5974–5985.
43 H. Gu, J. Guo, Q. He, Y. Jiang, Y. Huang, N. Haldolaarachige, Z. Luo, D. P. Young, S. Wei and Z. Guo, *Nanoscale*, 2014, **6**, 181–189.

44 P. Tao, A. Viswanath, L. S. Schadler, B. C. Benicewicz and R. W. Siegel, *ACS Appl. Mater. Interfaces*, 2011, **3**, 3638–3645.
45 C. D. Liu, S. N. Lee, C. H. Ho, J. L. Han and K. Hsieh, *J. Phys. Chem. C*, 2008, **112**, 15956–15960.
46 P. Herrasti, A. I. del Rio and J. Recio, *Electrochim. Acta*, 2007, **52**, 6496–6501.
47 J. Pendry, L. Martin-Moreno and F. Garcia-Vidal, *Science*, 2004, **305**, 847–848.
48 J. Homola, *Chem. Rev.*, 2008, **108**, 462–493.
49 J. B. Pendry, A. J. Holden, W. J. Stewart and I. Youngs, *Phys. Rev. Lett.*, 1996, **76**, 4773–4776.
50 M. Rashidi-Huyeh and B. Palpant, *Phys. Rev. B: Condens. Matter Mater. Phys.*, 2006, **74**, 075405.
51 G. S. Arnold, *Appl. Opt.*, 1984, **23**, 1434–1436.
52 P. B. Johnson and R. W. Christy, *Phys. Rev. B: Solid State*, 1972, **6**, 4370–4379.
53 J. S. Brooks, R. Vasic, A. Kismarahardja, E. Steven, T. Tokumoto, P. Schlottmann and S. Kelly, *Phys. Rev. B: Condens. Matter Mater. Phys.*, 2008, **78**, 045205.
54 S. R. Nagel and S. E. Schnatterly, *Phys. Rev. B: Solid State*, 1974, **9**, 1299–1303.
55 F. Capolino, *Theory and Phenomena of Metamaterials*, CRC Press, 2009.
56 P. Avouris and B. N. J. Persson, *J. Phys. Chem.*, 1984, **88**, 837–848.
57 A. B. Sproul and M. A. Green, *J. Appl. Phys.*, 1991, **70**, 846–854.
58 S. Hertel, D. Waldmann, J. Jobst, A. Albert, M. Albrecht, S. Reshanov, A. Schöner, M. Krieger and H. Weber, *Nat. Commun.*, 2012, **3**, 957.
59 B. I. Shklovskii, *Pis'ma Zh. Eksp. Teor. Fiz.*, 1982, **36**, 43 [*JETP Lett.*, **36**, 287, (1982)].
60 M. Aggarwal, S. Khan, M. Husain, T. Ming, M. Tsai, T. Perng and Z. Khan, *Eur. Phys. J. B*, 2007, **60**, 319–324.
61 L. Zhang and Z.-J. Tang, *Phys. Rev. B: Condens. Matter Mater. Phys.*, 2004, **70**, 174306.
62 C. Soukoulis and E. Economou, *Wave. Random Media*, 1999, **9**, 255–269.
63 J. P. Spatz, B. Lorenz, K. Weishaupt, H. D. Hochheimer, V. Menon, R. Parthasarathy, C. R. Martin, J. Bechtold and P.-H. Hor, *Phys. Rev. B: Condens. Matter Mater. Phys.*, 1994, **50**, 14888–14892.
64 Z. Guo, M. Moldovan, D. P. Young, L. L. Henry and E. J. Podlaha, *Electrochem. Solid-State Lett.*, 2007, **10**, E31–E35.
65 A. L. Lin, T. Wu, W. Chen and A. T. Wee, *Appl. Phys. Lett.*, 2013, **103**, 032408.
66 B. I. Shklovskii and A. L. Ėfros, *Electronic Properties of Doped Semiconductors*, Springer-Verlag, Appendix 3, 1984.